A Modified Radon Fourier Transform for GNSS-Based Bistatic Radar Target Detection

Xinkai Zhou, Pengbo Wang, *Member, IEEE*, Jie Chen, *Senior Member, IEEE*, Zhirong Men, *Member, IEEE*, Wei Liu, *Senior Member, IEEE*, and Hongcheng Zeng, *Member, IEEE*

***Abstract*— The Global Navigation Satellite System (GNSS)-based passive bistatic radar (PBR) which uses the GNSS signal as the illuminators of opportunity is studied for moving target detection (MTD). GNSS-based PBR has many advantages due to the removal of the transmitting device; however, its fundamental limitation is the low power density of the GNSS signal. Therefore, the integration time should be sufficiently long to obtain a promising maximum detectable range. On the other hand, the integration time is limited by the range migration and Doppler migration of the echo caused by target motion. In this letter, a novel MTD algorithm is proposed for the GNSS-based PBR, by employing a modified radon Fourier transform (MRFT) to achieve the required long-time integration for moving targets. The MRFT integrates the echo energy via joint searching of range, Doppler, and Doppler rate of the target, which can handle not only the range migration but also the Doppler migration problems, and significantly improves the signal-to-noise ratio (SNR) of the echo signal. An experiment using the GPS L5 signal as the illumination source is conducted and a moving car is successfully detected by the proposed algorithm, although significant range migration and Doppler migration are present due to variation of its speed.**

***Index Terms*— Global navigation satellite system (GNSS), long-time integration, modified radon Fourier transform (MRFT), moving target detection (MTD), passive bistatic radar (PBR).**

I. Introduction

SIGNALS transmitted by the Global Navigation Satellite System (GNSS) are being utilized in more and more remote sensing applications recently [1], with GNSS-Reflectometry (GNSS-R) being the most well-known technique. The applications of GNSS-R include the retrieval of ocean wind speed [2], soil moisture [3], and so on. Another technique is the GNSS-based bistatic synthetic aperture radar (SAR) [4], [5], which is suitable for Earth mapping and surveillance.

This letter focuses on the GNSS-based passive bistatic radar (PBR) for moving target detection (MTD), which has attracted increasing interest in the radar community [6]–[10]. It uses GNSS as illuminators of opportunity and due to the removal of transmitting devices, GNSS-based PBR has several significant advantages, such as low power, lightweight, and covert operations. It could also achieve global coverage since there will always be several GNSS satellites of each network (GPS, GLONASS, Galileo, or BeiDou) visible at any location on Earth's surface. Moreover, synchronization can be achieved conveniently with the aid of GNSS time service.

The concept of using the GNSS signal for MTD was first considered by Koch and Westphal [6]. Their early work demonstrated the ability of detecting various targets using GPS illuminators, including military and civilian aircrafts, an anti-tank missile, and the Mir Space Station, using a forward scatter geometry. The forward scatter geometry requires the target crossing the transmitter–receiver baseline, which is a rather restrictive condition. In [7], a GNSS-based PBR with a general bistatic geometry for maritime moving target indication was described. The performance of the system is preliminarily investigated and tested by an experiment to detect a lake ferry. As analyzed in [7], maritime surveillance is one of the potential applications of the GNSS-based PBR. For example, it could be deployed on a coastal hill to achieve long-term passive monitoring of the near ocean.

The fundamental limitation of the GNSS-based PBR is the low power density of the GNSS signal [10]. Generally, a large receiving antenna and a fairly long coherent integration time are required for the GNSS-based PBR to obtain a sufficient signal-to-noise ratio (SNR) for effective detection at a promising range. However, the motion of the target will cause range migration as well as Doppler migration of the echo during the coherent processing interval (CPI), which limits the integration length. In [7], a long-time integration algorithm for GNSS-based PBR is proposed, where the total processing interval is divided into several consecutive frames. Intraframe coherent integration and interframe noncoherent integration are performed to obtain the final focused range doppler (RD) image. In [8], the intraframe Doppler migration is further considered to enlarge the frame length. Those algorithms could effectively improve the SNR. However, since intraframe range migration is not considered, the coherent integration length would be limited for high-speed targets. Focus-before-detection (FBD) methods could achieve long-time coherent integration of weak target without prior knowledge of target motion parameters. One of the most well-known FBD method is the radon Fourier transform (RFT) [11]. The RFT can achieve long-time integration for target echo with significant range migration via joint searching of target range and velocity. However, it cannot handle the Doppler migration problem. The generalized RFT (GRFT) provides a general method for maneuvering target long-time coherent integration [12]. It could be applied to the GNSS-based PBR to deal with the Doppler migration problem, but its implementation needs an ergodic multidimensional search.

Manuscript received May 23, 2020; revised October 21, 2020; accepted November 17, 2020. This work was supported in part by the National Natural Science Foundation of China (NNSFC) under Grant 61861136008 and in part by the Beijing Natural Science Foundation under Grant 4194081. *(Corresponding author: Hongcheng Zeng.)*

Xinkai Zhou, Pengbo Wang, Jie Chen, Zhirong Men, and Hongcheng Zeng are with the School of Electronics and Information Engineering, Beihang University, Beijing 100191, China (e-mail: zhoux1nka1@buaa.edu.cn; wangpb7966@buaa.edu.cn; chenjie@buaa.edu.cn; menzhirong@buaa.edu.cn; zenghongcheng@buaa.edu.cn).

Wei Liu is with the Department of Electronic and Electrical Engineering, University of Sheffield, S1 3JD Sheffield, U.K. (e-mail: w.liu@sheffield.ac.uk).

Color versions of one or more figures in this article are available at https://doi.org/10.1109/LGRS.2020.3041623.

Digital Object Identifier 10.1109/LGRS.2020.3041623

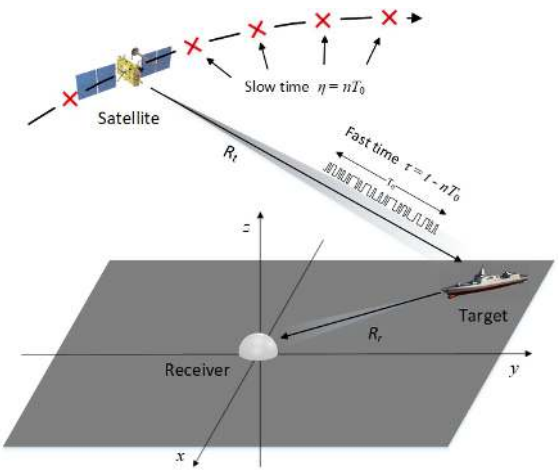

Fig. 1. General geometry of the GNSS-based PBR.

In this letter, the signal model of an arbitrarily moving target is established first for the GNSS-based PBR. Based on the signal model, a novel MTD algorithm is proposed by employing a modified RFT (MRFT) to realize the long-time coherent integration. Compared with the RFT, the MRFT adds a Doppler rate searching step during pulse integration, which can handle not only the range migration but also the Doppler migration problems and significantly increase the achievable integration time. Compared with the GRFT, the MRFT avoids the sample updating step for every searching Doppler rate, and hence is more efficient. Finally, an experiment is carried out to test the proposed algorithm. GPS L5 signal is chosen as the illumination source, with a moving car on the road as the target. Under the experimental settings, the car is successfully detected by the ground-based radar. Coherent integration is performed to the collected data with a CPI of 3 s. Due to deceleration of the car, both the range migration and Doppler migration of the echo are significant within the CPI. Aided by the MRFT step, a significant improvement in SNR is achieved, which confirms both the system concept and the feasibility of the proposed algorithm.

The rest of this letter is organized as follows: the signal model and a description of the proposed algorithm are presented in Section I. Experimental results are provided in Section III. Conclusions are drawn in Section IV.

II. Methodology

The general geometry of the GNSS-based PBR is shown in Fig. 1. The receiver is fixed on the ground. Two receiving channels are employed. The direct channel is used for GNSS tracking and positioning, whereas the reflect channel is used for target detection. Generally, GNSS signal can be thought of as the product of three-time waveforms [13]: the radio frequency (RF) carrier, the ranging code, and the navigation data. Under the "stop-and-go" assumption, the target echo after intermediate frequency (IF) demodulation could be expressed as

$$s(t) = A_m D(t) \sum_{n=0}^{Na-1} C\left(t - nT_0 - \frac{R(nT_0)}{c}\right) \times \exp\left(-j2\pi \frac{R(nT_0)}{\lambda}\right) \quad (1)$$

$$R(t) = R_t(t) + R_r(t) \quad (2)$$

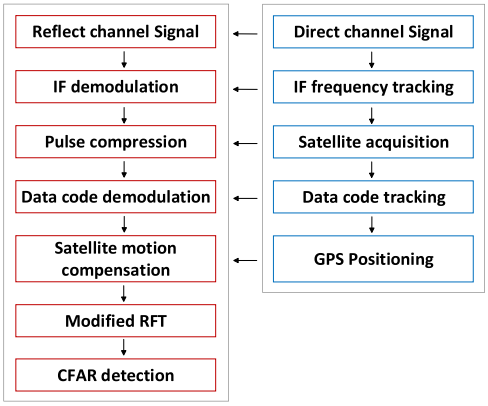

Fig. 2. Block diagram of the proposed algorithm.

where $D(\cdot)$ and $C(\cdot)$ are the data code and ranging code sequences, respectively, T_0 is the period of the ranging code, N_a is the number of pulses for integration, c is the speed of light, λ is the wavelength of the RF carrier, A_m is the amplitude of the signal, $R_t(t)$ is the range between the transmitter and the target, $R_r(t)$ is the range between the receiver and the target, and $R(t)$ is the total range.

The block diagram of the proposed algorithm is shown in Fig. 2. In general, it consists of a main signal processing flow (reflect channel) and a supplementary signal processing flow (direct channel).

Pulse compression is accomplished by the correlation between the target signal and the ranging code of the chosen satellite. After pulse compression, the signal can be expressed as

$$s(t) = A_m D(t) \sum_{n=0}^{Na-1} P\left(t - nT_0 - \frac{R(nT_0)}{c}\right) \times \exp\left(-j2\pi \frac{R(nT_0)}{\lambda}\right) \quad (3)$$

where $P(\cdot)$ is the autocorrelation function of the ranging code.

The data code carries the navigation message of the satellite, which acts as interference for radar and should be removed in advance. After data code demodulation, the signal becomes

$$s(t) = A_m \sum_{n=0}^{Na-1} P\left(t - nT_0 - \frac{R(nT_0)}{c}\right) \exp\left(-j2\pi \frac{R(nT_0)}{\lambda}\right). \quad (4)$$

The 2-D radar data matrix is then formed by storing the 1-D data flow of per ranging code period as one row

$$s(\eta, \tau) = A_m \mathrm{rect}\left[\frac{\eta - T_a/2}{T_a}\right] P\left(\tau - \frac{R(\eta)}{c}\right) \exp\left(-j2\pi \frac{R(\eta)}{\lambda}\right) \quad \eta \in [0,\ T_a],\quad \tau \in [0,\ T_0] \quad (5)$$

where $\eta = nT_0$ is the slow-time and $\tau = t - nT_0$ is the fast-time. And $T_a = N_a T_0$ is the CPI.

The range migration and Doppler phase of the echo are caused simultaneously by the satellite motion relative to the receiver which can be acquired by ephemeris data, and the target motion relative to the receiver which is unknown before target detection. Compensating the satellite motion first,

the signal becomes

$$s(\eta, \tau) = A_m \text{rect}\left[\frac{\eta}{T_a}\right] P\left(\tau - \frac{R(\eta) - R_{\text{ref}}(\eta)}{c}\right) \times \exp\left(-j2\pi \frac{R(\eta) - R_{\text{ref}}(\eta)}{\lambda}\right) \quad (6)$$

where R_{ref} is the range between the satellite and the receiver.

Expanding $R(\eta)$–$R_{\text{ref}}(\eta)$ at $\eta = 0$ and keeping only those up to the second order, we have

$$R(\eta) - R_{\text{ref}}(\eta) \approx R_0 - \lambda f_d \eta - 0.5\lambda f_r \eta^2 \quad (7)$$

$$R_0 = R(0) - R_{\text{ref}}(0) \quad (8)$$

where f_d and f_r are the Doppler and Doppler rate of the signal caused by target motion relative to the receiver, respectively. Substituting (7) into (6), we have

$$s(\eta, \tau) = A_m \text{rect}\left[\frac{\eta}{T_a}\right] P\left(\tau - \frac{R_0 - \lambda f_d \eta - 0.5\lambda f_r \eta^2}{c}\right) \times \exp\left(-j2\pi \frac{R_0}{\lambda} + j2\pi f_d \eta + j\pi f_r \eta^2\right). \quad (9)$$

Since the range resolution of the GNSS-based PBR is fairly poor (tens of meters or even hundreds of meters depending on the exploited GNSS channel), the quadratic term of the range migration is typically smaller than the resolution cell, and can be ignored. The constant term of the Doppler phase can also be omitted in (9) for simplicity. The signal then becomes

$$s(\eta, \tau) = A_m \text{rect}\left[\frac{\eta}{T_a}\right] P\left(\tau - \frac{R_0 - \lambda f_d \eta}{c}\right) \times \exp\left(j2\pi f_d \eta + j\pi f_r \eta^2\right) \quad (10)$$

or be expressed by parameter pair (η, R) as

$$s(\eta, R) = A_m rect\left[\frac{\eta}{T_a}\right] P\left(\frac{R - R_0 + \lambda f_d \eta}{c}\right) \times \exp\left(j2\pi f_d \eta + j\pi f_r \eta^2\right). \quad (11)$$

As can be seen from (11), the echo of a moving target is distributed along a straight line $R = R_0 - \lambda f_d \eta$ in the η-R plane, which represents the range migration, with a quadratic modulation $\varphi = \pi f_r \eta^2$ on the Doppler phase, which represents the Doppler migration. For the conventional MTD radar with high transmitting power, the needed integration time is relatively short, and those migrations are typically negligible compared with the range or Doppler resolutions. However, for the GNSS-based PBR which requires long-time integration, those migrations become significant, and limit the maximum integration time. In order to handle this problem, the MRFT is proposed here, which is defined as

$$S(R_0, f_d, f_r) = \int_{-T_a/2}^{T_a/2} s(\eta, R_0 - \lambda f_d \eta) \times \exp(-j\pi f_r \eta^2) \exp(-j2\pi f_d \eta) d\eta$$

$$R_0 \in [R_{\min}, R_{\max}], \quad f_d \in \left[-\frac{2v_{\max}}{\lambda}, \frac{2v_{\max}}{\lambda}\right],$$

$$f_r \in \left[0, -\frac{v_{\max}^2}{\lambda R_{\min}}\right] \quad (12)$$

where $R_{\min}$ and $R_{\max}$ are the minimum and maximum detection ranges, and $v_{\max}$ is the maximum velocity of the target.

The RFT was initially proposed to handle the range migration problem in conventional radar. It could integrate the echo energy with across range unit (ARU) range migration via joint search of target range and velocity. Compared with RFT, the MRFT adds a Doppler rate searching step which could solve not only the range migration but also the Doppler migration problem. A graphical illustration of the MRFT is shown in Fig. 3. Generally, the MRFT could be decomposed into three subsequent steps:

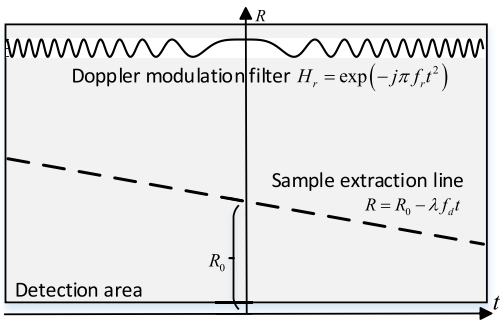

Fig. 3. Illustration of the MRFT.

First, extract samples along a straight line with respect to certain searching range R_0 and searching Doppler f_d. The equation of the sample extraction path is

$$R = R_0 - \lambda f_d \eta. \quad (13)$$

Second, perform Doppler modulation with respect to certain searching Doppler rate. The expression of the Doppler modulation filter is

$$H_r = \exp(-j\pi f_r \eta^2). \quad (14)$$

Third, complete coherent integration via the Fourier integration, and the Doppler function is

$$H_d = \exp(-j2\pi f_d \eta). \quad (15)$$

Obviously, when the searching parameters match the true values of target's range, Doppler, and Doppler rate, the echo energy distributed along multiple pulses will be coherently integrated, and generates a peak value

$$S(R_0, f_d, f_r)|_{\max} = S(R_0^*, f_d^*, f_r^*) = A_m T_a P_0 \quad (16)$$

where $P_0 = \text{P}(\tau)|\tau = 0$.

The SNR improvement added by the MRFT step is

$$G = |f_r T_a^2|. \quad (17)$$

Constant false-alarm rate (CFAR) detection could then be applied to detect the moving targets. The parameters estimated in the MRFT step could be used to compensate for target motion, and obtain the focused image of the target in the range-Doppler domain.

III. Experimental Results

The experiment was conducted near a road in Changping District, Beijing, China at 12:10 a.m. on May 19, 2019. An illustration of the experimental scene is shown in Fig. 4. The receiver was fixed on the ground by the road. The experimental setups are shown in Fig. 5. Some experimental parameters are listed in Table I. The beam of the reflect channel antenna is pointed toward the car, and the direct channel has a standard GPS L1/L5 double-frequency antenna pointing toward the sky. The GPS satellite PRN1 is chosen as the illumination source.

Fig. 4. Illustration of the experimental scene.

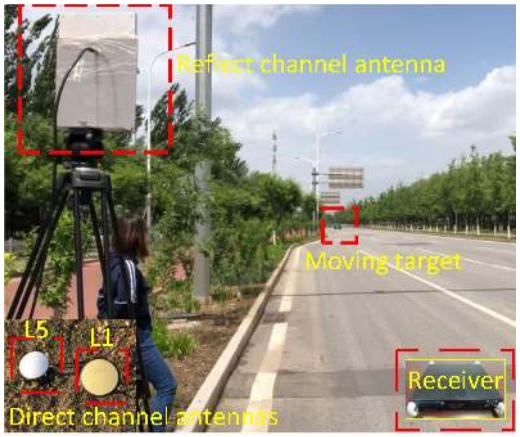

Fig. 5. Experimental setups.

TABLE I
SOME EXPERIMENTAL PARAMETERS

Quantity	Value	Quantity	Value
Satellite	GPS PRN1	Signal Bandwidth	10.23MHz
Satellite signal	L5	Equivalent PRF	1000Hz
Satellite elevation	18°	Sampling rate	62MHz
Carrier frequency	1176.45MHz	Antenna gain	10dB

The target is successfully detected by applying the proposed algorithm to the collected data. The range compressed result of the reflect channel data after satellite motion compensation is shown in Fig. 6. As can be seen, the trajectory of the car in a 3-second duration is clearly identified (note that to reveal the target's trajectory, the data has been low-pass filtered in the Doppler domain with a cutoff frequency of 150 Hz to smooth the noise). Since the range migration caused by satellite motion has already been corrected at this step, the residual range migration in Fig. 6 is mainly caused by target motion. The range-Doppler domain result of the 3-s data is shown in Fig. 7. As can be seen, due to deceleration of the car, both the range migration and the Doppler migration of the echo are significant. The echo energy is no longer positioned in the same range unit, and the slow-time data sequence is also not a complex sinusoid. Obviously, in this case, neither the conventional pulse-Doppler processing nor the RFT algorithm could realize coherent integration of the echo energy.

The Doppler bandwidth of ground clutter is about 1.5 Hz, and those clutter power should be filtered out first before

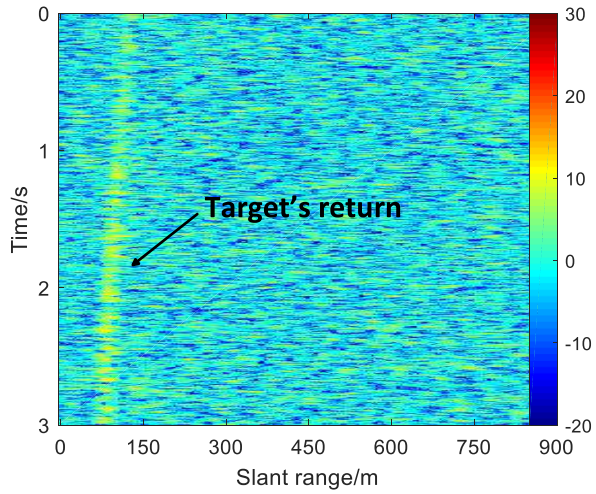

Fig. 6. Range compressed result after satellite motion compensation (the amplitude has been normalized to the mean noise power level).

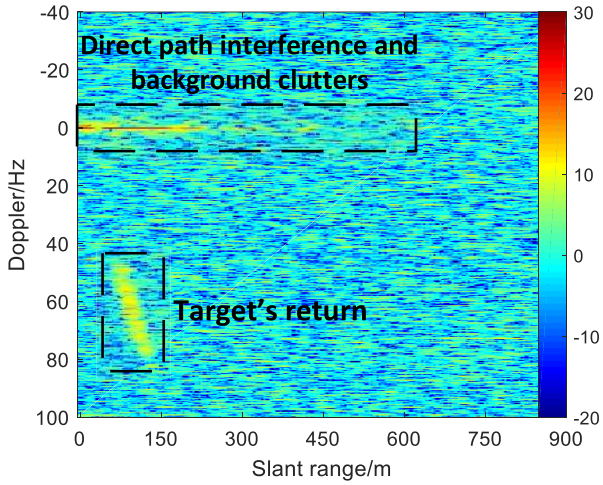

Fig. 7. Range-Doppler domain result (the amplitude has been normalized to the mean noise power level).

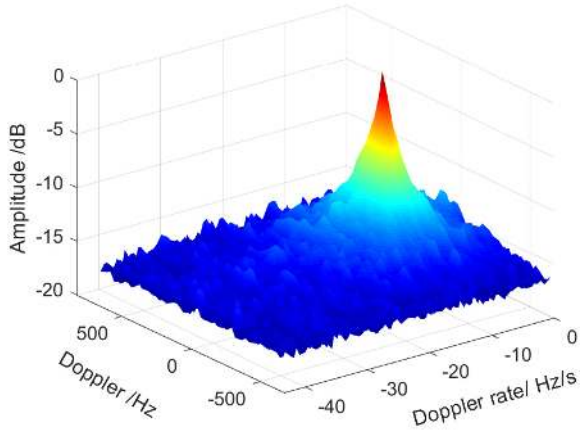

Fig. 8. Slice of the MRFT result at $R_0 = R_0^*$ (the amplitude has been normalized to its maximum value).

detection. The MRFT is then performed to show its ability in handling the range and Doppler migration problems for long-time integration. Fig. 8 shows the MRFT result of the echo data with a CPI of 3 s (slice along Doppler and Doppler rate dimensions at $R_0 = R_0^*$). The peak value of the MRFT

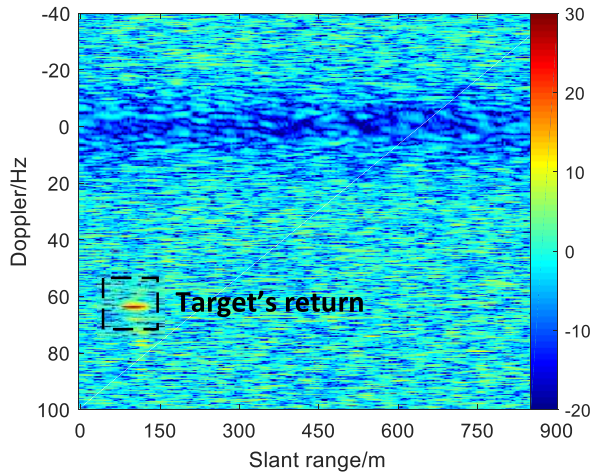

Fig. 9. Range-Doppler result after target motion compensation (the amplitude has been normalized to the mean noise power level).

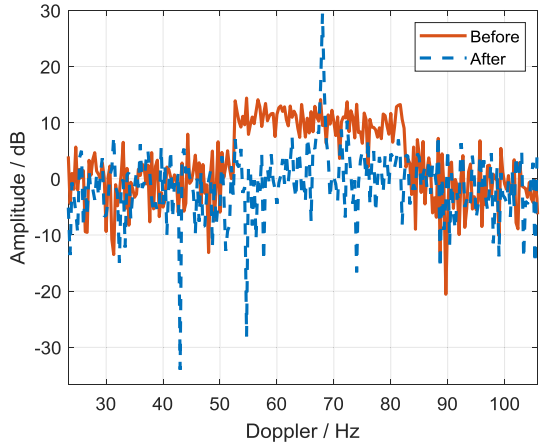

Fig. 10. Comparison between the Doppler profiles before and after target motion compensation.

TABLE II
ESTIMATED PARAMETERS OF THE CAR

Parameter	Estimated value
Central slant range	96m
Central Doppler	68Hz
Doppler rate	-10Hz/s

is just the coherent integration result of the data. The range, Doppler, and Doppler rate corresponding to this peak value are chosen as the estimated parameters of the target, as listed in Table II. To demonstrate the ability of the MRFT in improving SNR more effectively, the range-Doppler domain result of the data after target motion compensation using the estimated parameters is shown in Fig. 9. Compared with Fig. 7, a significant improvement on SNR can be observed in Fig. 9, and the echo energy is well focused. The Doppler profiles of the target before and after motion compensation are plotted together in Fig. 10 for comparison. The theoretical and measured values of the SNR improvement added by the MRFT step are listed in Table III. It can be observed that the SNR has increased by 16.4 dB, confirming the feasibility of the MRFT for long-time integration of the GNSS-based PBR. There is a 3.1 dB difference in the theoretical and measured

TABLE III
SNR IMPROVEMENT

Measured value	Theoretical value
16.4dB	19.5dB

SNR improvement values, which may be caused by the variation of signal amplitude, parameter estimation errors, and the variation of target deceleration.

IV. CONCLUSION

In this letter, to handle the range migration and Doppler migration problems for long-time integration in GNSS-based PBR, a novel MTD algorithm has been presented. The key step is an MRFT which significantly improves the maximum integration time via joint search of range, Doppler, and Doppler rate of the target. To verify the feasibility of the proposed MTD algorithm and demonstrate the performance of the MRFT in long-time integration, one set of data was successfully recorded with a moving car as the target. The obtained MTD results have clearly identified the motion of the car, which coincide with the ground truth. Significant improvement in SNR has also been achieved by the MRFT step, further confirming the effectiveness of the MRFT in long-time integration.

REFERENCES

[1] V. U. Zavorotny, S. Gleason, E. Cardellach, and A. Camps, "Tutorial on remote sensing using GNSS bistatic radar of opportunity," *IEEE Geosci. Remote Sens. Mag.*, vol. 2, no. 4, pp. 8–45, Dec. 2014.

[2] G. Foti *et al.*, "Spaceborne GNSS reflectometry for ocean winds: First results from the UK TechDemoSat-1 mission," *Geophys. Res. Lett.*, vol. 42, no. 13, pp. 5435–5441, Jul. 2015.

[3] N. Rodriguez-Alvarez *et al.*, "Soil moisture retrieval using GNSS-R techniques: Experimental results over a bare soil field," *IEEE Trans. Geosci. Remote Sens.*, vol. 47, no. 11, pp. 3616–3624, Nov. 2009.

[4] M. Cherniakov *et al.*, "Space-surface bistatic synthetic aperture radar with global navigation satellite system transmitter of opportunity-experimental results," *IET Radar Sonar Navig.*, vol. 1, no. 6, pp. 447–458, Dec. 2007.

[5] F. Santi, M. Antoniou, and D. Pastina, "Point spread function analysis for GNSS-based multistatic SAR," *IEEE Geosci. Remote Sens. Lett.*, vol. 12, no. 2, pp. 304–308, Feb. 2015.

[6] V. Koch and R. Westphal, "New approach to a multistatic passive radar sensor for air/space defense," *IEEE Aerosp. Electron. Syst. Mag.*, vol. 10, no. 11, pp. 24–32, Nov. 1995.

[7] H. Ma *et al.*, "Maritime moving target indication using passive GNSS-based bistatic radar," *IEEE Trans. Aerosp. Electron. Syst.*, vol. 54, no. 1, pp. 115–130, Feb. 2018.

[8] D. Pastina *et al.*, "Maritime moving target long time integration for GNSS-based passive bistatic radar," *IEEE Trans. Aerosp. Electron. Syst.*, vol. 54, no. 6, pp. 3060–3083, Dec. 2018.

[9] F. Santi, F. Pieralice, and D. Pastina, "Joint detection and localization of vessels at sea with a GNSS-based multistatic radar," *IEEE Trans. Geosci. Remote Sens.*, vol. 57, no. 8, pp. 5894–5913, Aug. 2019.

[10] C. V. Ilioudis *et al.*, "GNSS based passive radar for UAV monitoring," in *Proc. IEEE Radar Conf.*, Boston, MA, USA, Sep. 2019, pp. 1–6.

[11] J. Xu, J. Yu, Y.-N. Peng, and X.-G. Xia, "Radon-Fourier transform for radar target detection, I: Generalized Doppler filter bank," *IEEE Trans. Aerosp. Electron. Syst.*, vol. 47, no. 2, pp. 1186–1202, Apr. 2011.

[12] J. Xu, X.-G. Xia, S.-B. Peng, J. Yu, Y.-N. Peng, and L.-C. Qian, "Radar maneuvering target motion estimation based on generalized radon-Fourier transform," *IEEE Trans. Signal Process.*, vol. 60, no. 12, pp. 6190–6201, Dec. 2012.

[13] D. K. Elliott and H. Chris, "GPS satellite signal characteristics," in *Understanding GPS: Principles and Applications*, 2nd ed. Fitchburg, MA, USA: Artech House, 2005, ch. 4, sec. 2, pp. 114–115.